A&A 599, A81 (2017)
DOI: 10.1051/0004-6361/201630030

Astronomy & Astrophysics

OmegaWINGS: spectroscopy in the outskirts of local clusters of galaxies⋆

A. Moretti[1], M. Gullieuszik[1], B. Poggianti[1], A. Paccagnella[1,2], W. J. Couch[3], B. Vulcani[4], D. Bettoni[1], J. Fritz[5], A. Cava[6], G. Fasano[1], M. D'Onofrio[1,2], and A. Omizzolo[1,7]

[1] INAF–Osservatorio astronomico di Padova, Vicolo dell'Osservatorio 5, 35122 Padova, Italy
e-mail: alessia.moretti@oapd.inaf.it
[2] Dipartimento di Fisica e Astronomia, Università degli Studi di Padova, Vicolo dell'Osservatorio 3, 35122 Padova, Italy
[3] Australian Astronomical Observatory, PO Box 915, North Ryde, NSW 1670, Australia
[4] School of Physics, University of Melbourne, Melbourne VIC 3010, Australia
[5] Instituto de Radioastronomía y Astrofísica, UNAM, Campus Morelia, A.P. 3-72, 58089 Morelia, Mexico
[6] Observatoire de Genève, Université de Genève, 51 Ch. des Maillettes, 1290 Versoix, Switzerland
[7] Specola Vaticana, 00120, Vatican City State, Italy

Received 8 November 2016 / Accepted 22 December 2016

ABSTRACT

Context. Studies of the properties of low-redshift cluster galaxies suffer, in general, from small spatial coverage of the cluster area. WINGS, the most homogeneous and complete study of galaxies in dense environments to date, obtained spectroscopic redshifts for 48 clusters at a median redshift of 0.05, out to an average distance of approximately 0.5 cluster virial radii. The WINGS photometric survey was recently extended by the VST survey OmegaWINGS to cover the outskirts of a subset of the original cluster sample.
Aims. In this work, we present the spectroscopic follow-up of 33 of the 46 clusters of galaxies observed with VST over 1 square degree. The aim of this spectroscopic survey is to enlarge the number of cluster members and study the galaxy characteristics and the cluster dynamical properties out to large radii, reaching the virial radius and beyond.
Methods. We used the AAOmega spectrograph at AAT to obtain fiber-integrated spectra covering the wavelength region between 3800 and 9000 Å with a spectral resolution of 3.5−6 Å full width at half maximum (FWHM). Observations were performed using two different configurations and exposure times per cluster. We measured redshifts using both absorption and emission lines and used them to derive the cluster redshifts and velocity dispersions.
Results. We present here the redshift measurements for 17 985 galaxies, 7497 of which turned out to be cluster members. The sample magnitude completeness is 80% at $V = 20$. Thanks to the observing strategy, the radial completeness turned out to be relatively constant (90%) within the AAOmega field of view. The success rate in measuring redshifts is 95%, at all radii.
Conclusions. We provide redshifts for the full sample of galaxies in OmegaWINGS clusters together with updated and robust cluster redshift and velocity dispersions. These data, publicly accessible through the CDS and VO archives, will enable evolutionary and environmental studies of cluster properties, providing a local benchmark.

Key words. galaxies: clusters: general – galaxies: distances and redshifts

1. Introduction

The WINGS survey (Fasano et al. 2006) was the first attempt to map local galaxy clusters (median redshift ∼0.05, 76 clusters) over a wide field of view in the optical range. With respect to other surveys of nearby galaxies, such as the Sloan Digital Sky Survey (SDSS; York 2000), it offers the advantage of being targeted to X-ray-selected clusters. Moreover, it reaches galaxy magnitudes that are 1.5 mag deeper than the ones obtained by the widely used SDSS.

The WINGS survey was extended in the near IR (Valentinuzzi et al. 2009) for 28 clusters using data collected with the WFCAM camera at the UKIRT, covering a region four times larger than the optical one.

The spectroscopic follow-up (Cava et al. 2009) allowed the measurement of approximately 6000 new redshifts in 48 out of the 76 clusters and the determination of accurate velocity dispersions and membership. Only 21/48 clusters, though, had at least 50% completeness and could be used in statistical studies (Valentinuzzi et al. 2010; Vulcani et al. 2011a,b, 2012; Moretti et al. 2015). The complete set of measurements made on the WINGS dataset is available using the Virtual Observatory tool (Moretti et al. 2014).

The WINGS coverage of $\sim 30 \times 30$ arcmin^2 often covers just half of the cluster virial radius, and is thus missing the more external regions of the clusters. This represents a serious limitation for the comprehension of galaxy formation in clusters, as the cluster outskirts are the regions where galaxies probably undergo the major transformations that reflect, for instance, into the well known morphology-density relation (Dressler 1980). In particular, Fasano et al. (2015), using the WINGS dataset, found that this relation seems to disappear outside of the cluster core, supporting the notion that the relation between the morphological mix of galaxies and the distance from the cluster center might be more prominent than that with local density in these regions. Several other studies have pointed out the dependence

⋆ The complete catalog of OmegaWINGS redshift is available at the CDS via anonymous ftp to cdsarc.u-strasbg.fr (130.79.128.5) or via
http://cdsarc.u-strasbg.fr/viz-bin/qcat?J/A+A/599/A81

of galaxy properties on cluster-centric radius also at large distances (Lewis et al. 2002; Gomez et al. 2003).

Moreover, studies on cluster luminosity functions (LF) highlighted how, when comparing LFs in different clusters, it is mandatory to compare the same physical regions (Popesso et al. 2006; Barkhouse et al. 2007; Moretti et al. 2015), which, so far, have always been restricted to $0.5R_{200}$.

Cluster outskirts are the places where galaxies are either individually accreted, or processed in groups and filaments that eventually fall into the cluster potential, and therefore represent the transition region where galaxy transformations take place (Lewis et al. 2002; Pimbblet et al. 2001; Moran et al. 2007).

This specific transition region has been studied in detail in a few single clusters and superclusters (Merluzzi et al. 2010; Haines et al. 2011; Jaffé et al. 2011; Smith et al. 2012; Merluzzi et al. 2014), but, up to now, a systematic study of cluster outskirts has been hampered by the lack of an appropriate set of observational data.

Very recently, the WINGS survey has been extended with OMEGACAM at VST (Gullieuszik et al. 2015), with the aim of covering the virial radius of the observed clusters. The OmegaWINGS photometric survey covers 57 out of the original 76 clusters (among those with ($\delta \leq 20^{\circ}$), visible with the VST).

The OmegaWINGS sample of cluster galaxies has already been used to investigate properties of transition galaxies out to the virial radius and beyond and led to the discovery of a widespread population of galaxies with suppressed Specific Star Formation Rate (SSFR), possibly undergoing a slow quenching of star formation (Paccagnella et al. 2016).

This paper describes the spectroscopic follow-up of the OmegaWINGS survey. Section 2 describes the sample and the target selection criteria, Sect. 3 describes the spectroscopic observations and data reduction, while in Sect. 4, we assess the data quality, including the signal to noise and the completeness. In Sect. 5, we illustrate the redshift measurement procedure, and in Sect. 6, we give the principal products of the spectroscopic catalog, that is, velocity dispersions and memberships. Finally, in Sect. 7, we describe how to access the entire set of measurements. A short summary is given then in Sect. 8.

2. Sample and survey strategy

The OmegaWINGS spectroscopic survey is based on the photometric observations of 46 clusters (out of the 57 original OmegaWINGS sample).

The VST images, both in the V and B bands, cover a region of approximately 1 deg^2 around the cluster center, as derived from the SIMBAD database (Wenger et al. 2000), and are 50% complete at $V \sim 23$ mag. More important for the spectroscopic survey purposes is the internal accuracy of the astrometric calibration, that is equal to or better than $0.1''$.

The selection of candidates for the spectroscopic follow up was made using the OmegaWINGS photometric catalogs by Gullieuszik et al. (2015) on the basis of object magnitude and color. We selected the detections classified as galaxies with a total (Sextractor AUTO) magnitude brighter than $V = 20$ mag, and subsequently divided this sample into *bright* and *faint* sources according to their V aperture magnitude inside the fiber diameter ($2''.16$). Bright sources have $V_{\rm fib} \leq 20.5$ mag and faint sources have $20.5 \leq V_{\rm fib} \leq 21.5$. For each cluster, we therefore obtained two complementary sets of observations: one that has been exposed for 60 min, called *bright* configuration, and a second one, called *faint* configuration, with an exposure time of 120 min.

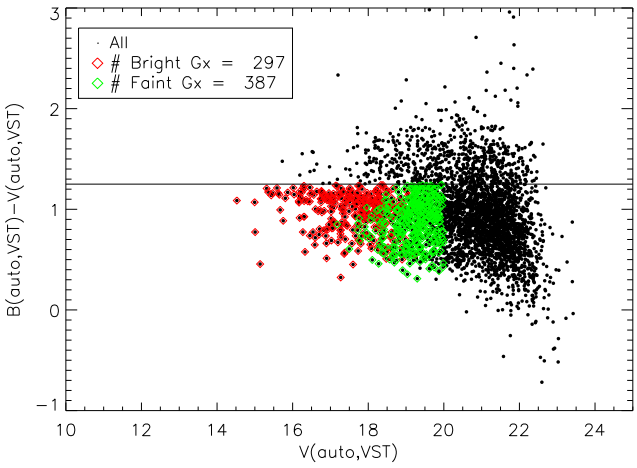

Fig. 1. Candidates for spectroscopic follow-up in A2382: the color cut is set at $(B - V) = 1.25$. Black dots are sources flagged as galaxies and red and green symbols indicate galaxies belonging to the *bright* and *faint* configurations, respectively.

To minimize the contamination from background galaxies, we applied a color cut to exclude extremely red background sources. This cut was set for each cluster by visually inspecting the color-magnitude diagram, in order to account for redshift variations, but in all cases, the color limit was very close to $B - V = 1.20$ mag. Finally, we assigned a priority to the targets. The targets located outside the original WINGS area had the highest priority, followed by the targets located inside the WINGS images but without a spectrum (intermediate priority), and by the targets located inside the WINGS region and with a previously determined redshift (lowest priority).

As an example, Fig. 1 shows the target selection for the cluster A2382: the black dots are sources from Gullieuszik et al. (2015) that have been classified as galaxies from the photometric survey, red points are galaxies belonging to the *bright* configuration, while green dots are galaxies belonging to the *faint* configuration.

3. Observations and data reduction

We used the AAOmega spectrograph (Smith et al. 2004; Sharp et al. 2006) at the Australian Astronomical Observatory (AAT), which can host up to 392 fibers over 2×2 deg^2. The fiber diameter is $2.16''$. The AAOmega spectrograph allows one to simultaneously take the blue and the red spectra of a target galaxy, using different grisms. In particular, we used the 580V and the 385R grisms, which have a resolution $R = 1300$ ($FWHM = 3.5$–6 Å). The observed wavelength range is ~3800–9000 Å.

For all configurations, we used 25 sky fibers, and 6 fibers for the guide stars, therefore we had ~360 available science fibers left per configuration. The positions of the sky fibers were chosen by visually inspecting OmegaWINGS images and looking for 25 regions with no sources, uniformly distributed over the entire field of view. Science targets were then positioned on the field by using the *configure* software, which takes into account the priorities described in Sect. 3 using a Simulated Annealing (SA) algorithm (Miszalski et al. 2006). A tumbling mechanism with two field plates allows the next field to be configured while the current field is being observed.

Observations started in August 2013 and were carried out in five different runs. Table 1 contains the number of nights in

Table 1. Observations.

Run	Nights	Targets	Success rate
August 2013	6	10 + 2	97.2 %
December 2013	3	5 + 3	89.0 %
July 2014	2	2 + 2	97.4 %
January 2015	5	4 + 4	92.8 %
September 2015	2	3 + 5	95.6 %

Notes. Number of observing nights, number of observed targets with both *faint* and *bright* configurations plus the number of configurations not completed, and average success rate of redshift measurements for each observational run.

the run, the number of observed targets for which we observed both configurations plus the number of configurations partially observed (either the *bright* or the *faint*), and the total success rate (i.e., the rate of successful redshift measurements over the total of assigned fibers in the run).

Some observations were carried out under non-optimal weather conditions; in some cases we therefore decided to increase the total exposure time to reach a sufficient signal-to-noise ratio for all targets. The detailed observing log for each configuration is shown in Table 2 where we also report the seeing and the percentage of observed galaxies for which we could obtain reliable redshift measurements (i.e., success rate in the last column). Some faint configurations (A168F, A3530F, A754F) could be exposed only for 1 h, therefore obtaining spectra with a low S/N (<5), which translates to a lower success rate. Arc exposures were taken before and after the scientific exposures. Moreover, for the faint configurations, we always also observed arc frames in between the science exposures, in order to properly calibrate in wavelength. The cluster A3266 has a second, deeper faint configuration that has been exposed for 18 000 s. With these observations, we enlarged the number of WINGS clusters with spectroscopic follow-up, adding the clusters A85, A168, A2717, A2734, A3532, A3528, A3530, A3558, A3667, A3716, A3880, and A4059.

The data reduction was performed using the dedicated pipeline *2dfdr*[1], which properly handles science and calibration (flat-field and arc) exposures, producing wavelength-calibrated spectra for each arm. After producing the single blue and red arm corrected spectra, we spliced them together using the region in common (at ~5700 Å) in order to get a single spectrum covering the entire observed spectral range. The spectra were corrected for the instrument sensitivity by the pipeline, while a proper flux calibration is missing. For the purpose of the spectro-photometric analysis (that will be presented in a forthcoming paper), we performed a relative flux calibration using a set of spectra in common with the SDSS. The sky subtraction was performed using the dedicated algorithm by Sharp & Parkinson (2010), that implements the Principal Component Analysis to derive an optimal sky estimate starting from dedicated sky exposures.

4. Data quality

We estimated the signal to noise ratios of the 17 985 AAOmega spectra averaged over the entire spectrum from the root mean square (rms) of the spectrum itself[2], obtaining values that go from approximately 11 to 16 (median and mean, respectively) for the bright configurations and from approximately 6 to 6 for

[1] https://www.aao.gov.au/science/software/2dfdr
[2] http://www.stecf.org/software/ASTROsoft/DER_SNR

Table 2. Observations log.

Cluster/Conf.	Run	Seeing [arcsec]	Exp. time [s]	Success rate
A1069 B	Dec. 13	2.0	3600	95
A1069 F	Dec. 13	1.8	6600	92
A151 B	Jan. 15	1.5	3600	96
A151 F	Jan. 15	1.8	7200	98
A1631a B	Jul. 14	1.5	3600	99
A1631a F	Jul. 14	1.6	7200	93
A168 B	Dec. 13	1.8	3600	79
A168 F	Dec. 13	1.5	3600	77
A193 B	Dec. 13	1.6	3600	100
A193 F	Sep. 15	1.9	6000	100
A2382 B	Aug. 13	1.5	3600	100
A2382 F	Aug. 13	1.3	7200	97
A2399 B	Aug. 13	1.3	3600	97
A2399 F	Aug. 13	1.5	7200	91
A2415 B	Sep. 15	2.1	3600	92
A2415 F	Sep. 15	1.7	7200	99
A2457 B	Aug. 13	4.2	3600	99
A2457 F	Aug. 13	3.0	7200	100
A2717 B	Sep. 15	1.4	3600	99
A2717 F	Jul. 14	1.3	7200	94
A2734 B	Sep. 15	2.4	3600	87
A2734 F	Sep. 15	1.5	7200	93
A3128 B	Aug. 13	1.1	3600	100
A3128 F	Aug. 13	1.4	7200	99
A3158 B	Aug. 13	1.5	3600	100
A3158 F	Aug. 13	1.3	7200	99
A3266 B	Aug. 13	1.3	3600	100
A3266 F	Aug. 13	3.5	7200	89
A3266 F*	Jan. 15	1.8	18 000	82
A3376 B	Jan. 15	3.2	3600	92
A3376 F	Jan. 15	1.6	7200	98
A3395 B	Dec. 13	1.6	3600	96
A3395 F	Dec. 13	1.6	7200	97
A3528 B	Jan. 15	2.2	3600	99
A3528 F	Jan. 15	1.7	7200	86
A3530 B	Dec. 13	2.5	3600	96
A3530 F	Dec. 13	2.2	3600	67
A3532 F	Jan. 15	1.5	7200	88
A3556 B	Aug. 13	1.6	3600	98
A3556 F	Aug. 13	1.3	7200	97
A3558 B	Jul. 14	1.5	3600	99
A3558 F	Aug. 13	1.5	7200	99
A3560 B	Jan. 15	1.8	3600	98
A3560 F	Jan. 15	1.6	7200	88
A3667 B	Aug. 13	1.2	3600	98
A3667 F	Aug. 13	1.4	7200	96
A3716 B	Aug. 13	3.0	3600	95
A3716 F	Aug. 13	1.3	7200	94
A3809 B	Jul. 14	1.2	3600	100
A3809 F	Jul. 14	1.6	7200	100
A3880 B	Aug. 13	0.7	3600	98
A3880 F	Aug. 13	1.0	7200	96
A4059 B	Sep. 15	1.7	3600	99
A4059 F	Sep. 15	1.8	7200	97
A500 B	Dec. 13	1.8	5500	98
A500 F	Dec. 13	1.6	7200	96
A754 B	Jan. 15	3.2	3600	89
A754 F	Dec. 13	1.4	7200	70
A85 B	Sep. 15	2.0	2400	99
A957 B	Jan. 15	1.3	3600	96
A970 B	Dec. 13	3.5	3600	96
A970 F	Jan. 15	1.8	12 000	90
IIZW108 B	Aug. 13	1.9	3600	99
IIZW108 F	Sep. 15	1.4	7200	86

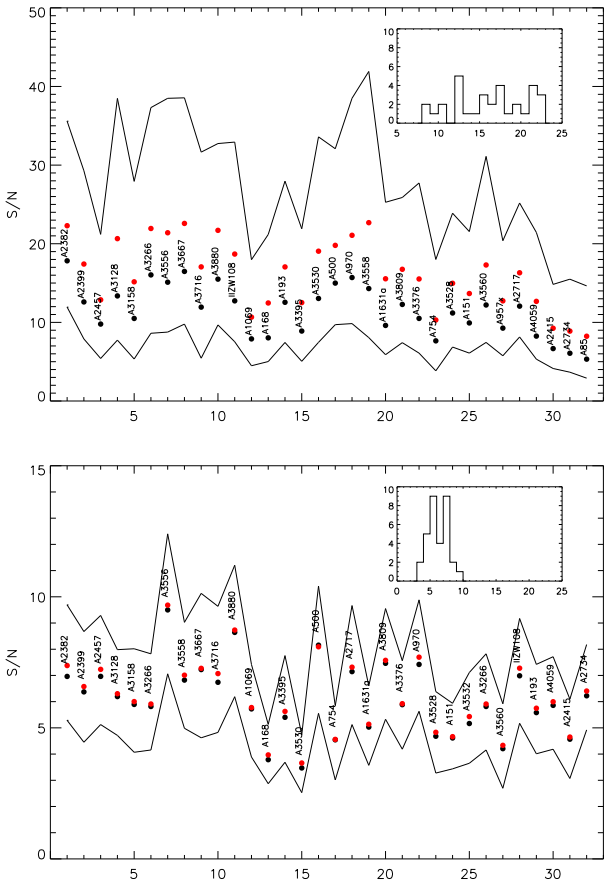

Fig. 2. Mean (red) and median (black) signal-to-noise together with the 68% confidence limits for the *bright* (*top panel*) and *faint* (*bottom panel*) configurations. In the *insets*, the average distributions of the measured signal-to-noise in the observed configurations (32 are bright and 32 are faint) are shown.

the faint configurations. Figure 2 shows the mean (in red) and the median (in black) signal to noise ratio together with the 68% confidence limit for the observed configurations.

The distributions of the average signal to noise (shown in the insets) reflect the objects magnitude range of the two configurations, with the bright configurations showing a larger range of measured S/N than the faint configurations.

As an example, in Fig. 3, we show two sets of observed spectra, belonging to the *bright* (top panel) and *faint* (bottom panel) configurations of A2382. The signal to noise ratio ranges from 55 to 15 in the brightest sources, while it goes down to 4 for the faintest ones. However, even for the faintest sources, we have been able to measure a redshift (see Sect. 5), mainly from emission lines. The spectra shown are those covering the entire AAOmega spectral range, that is, the ones obtained by combining the red and the blue arm of the spectrograph. Due to the small overlap in the common region, the combination turns out to be non-optimal for the continuum match, even though it does not hamper the redshift determination. Three spectral regions are clearly affected by dead pixels ([4660–4720 Å], [5258–5300 Å], [5560–5600 Å]).

5. Redshifts

We measured galaxy redshifts on the spliced spectra, that is, those extending over the entire wavelength range (3800–9000 Å), in order to gather information both from the blue part of the spectra (where at our redshifts, most optical absorption lines are present) and from the red part of the spectra (where the H_α + NII region is located). The night sky residuals, present in specific regions of the spectra, have been replaced by interpolated values before measuring the redshifts. On these cleaned spectra we measured both the redshift obtained by cross-correlating the spectrum with that of a template at zero velocity (using the *IRAF/xcsao* package) and the one obtained from the match of emission lines (*IRAF/emsao*).

Each single spectrum was visually inspected by members of the team (A.M., B.P., D.B., J.F., M.G., A.P., A.C.) to ensure that the automatic estimation was correct, and to assign a flag that was then used to derive the final redshift determination. We used:

- the weighted average of the two determinations if both were flagged as good;
- the emission line redshift if the cross-correlation was not convincing; and
- the cross-correlation redshift if spectra did not contain emission lines (and the cross correlation was reliable).

Errors on the redshifts are the errors of the combined measurements of both absorption features and emission features if the two redshift estimates were averaged together, and are single errors on the measurements that do not have emission lines, or where we did not trust the absorption line cross-correlation. Among the original 18 995 spectra, we were able to measure 17 985 redshifts, with a median error of 50 km s^{-1} and average completeness ~95%.

Figure 4 shows the distribution in redshift of all the OmegaWINGS targets (black line). The filled histogram represents the redshift determinations obtained with the previous WINGS spectroscopic survey (Cava et al. 2009), all in the inner cluster regions. The red histogram shows the new Omega WINGS redshifts. When a new redshift was present, we used this determination instead of the old WINGS one (the difference between the two determinations being peaked at 0, with a few cases of real mismatches in spectra with low S/N). The number of cluster members with a AAOmega redshift is 7497, that adds to the 2732 galaxies belonging to the clusters for which we had a previous WINGS measurement. This means that the total number of cluster members rises to 10 229 in total.

5.1. Completeness

To ensure that we could properly derive global properties from the clusters under scrutiny, and from their galaxy populations, we calculated the spectroscopic completeness as a function of both magnitude and radial distance. The first term C_m is calculated as

$$C(m) = \frac{N_z(m)}{N_{\rm ph}(m)}, \quad (1)$$

and gives, as a function of magnitude, the number of targets with a measured redshift ($N_z(m)$) with respect to the number of target galaxies in the same magnitude bin present in the parent photometric catalog ($N_{\rm ph}(m)$), that is, the photometric catalog from which we selected our spectroscopic target for the follow-up.

Recall that the candidates have to obey the following conditions:

- be classified as galaxies;
- have a V total magnitude brighter than $V = 20$ mag; and
- have a $(B - V)$ color bluer than the one defined by the cluster red sequence.

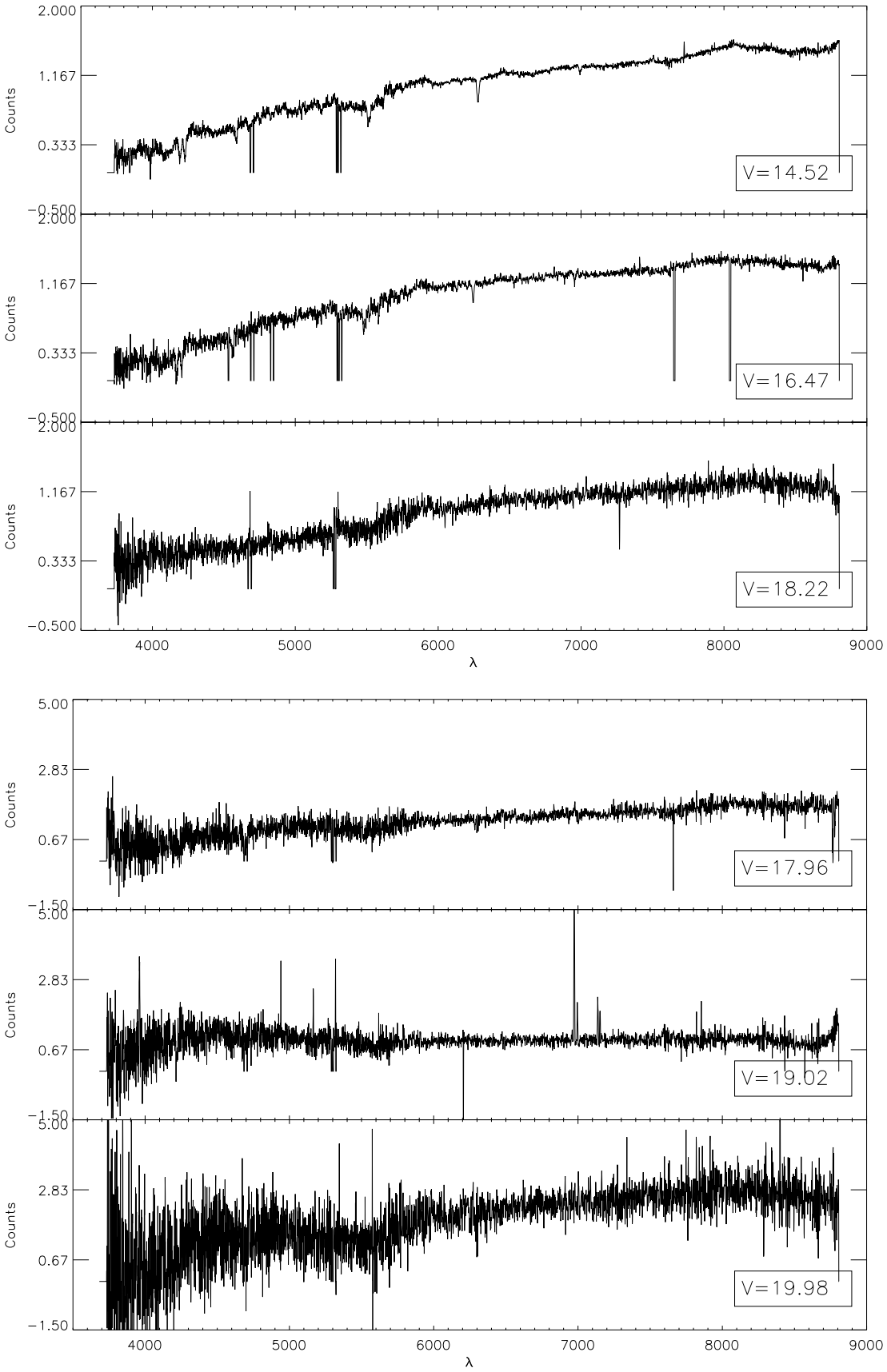

Fig. 3. Examples of observed spectra in the cluster A2382. *Upper panel* spectra belong to the *bright* configuration, while *lower panel* spectra belong to the *faint* configuration. *V* total magnitude is in the bottom right inset. The overall S/N is 55, 39, and 15 for the bright spectra, and 9, 6, and 4 for the faint ones.

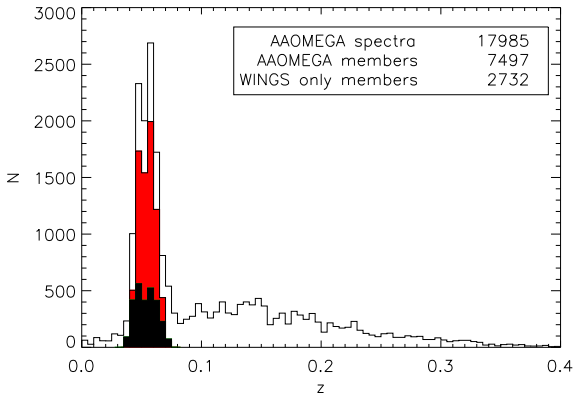

Fig. 4. Redshift distribution of OmegaWINGS targets: the empty histogram shows all redshifts and the red histogram shows the cluster members. The black histogram shows cluster members with a previous WINGS redshift that have not been re-observed with AAOmega.

The red sequence color varies slightly among clusters, and we took into account this effect in calculating the magnitude completeness. As for the radial completeness, we calculated it as the ratio between the number of targets with redshift with respect to the number of candidates in the parent photometric catalog in the same radial bin , that is,

$$C(r) = \frac{N_z(r)}{N_{\rm ph}(r)}, \tag{2}$$

where radial bins have been chosen to have the same area.

Figure 5 shows, from top to bottom, the success rate of redshift measurements as a function of the V magnitude, the completeness in magnitude, and the radial completeness expressed in terms of R/R_{200}.

The upper panel of Fig. 5 shows the success rate of the OmegaWINGS spectroscopic sample as a function of the total V magnitude of the targets, calculated as

$$S(m) = \frac{N_z(m)}{N_{\rm targ}(m)}, \tag{3}$$

and shows that at each magnitude bin, we were able to successfully measure redshifts in at least 90% of targets.

While the completeness in magnitude (middle panel of Fig. 5) decreases at fainter luminosities, reaching a value of 80% at $V = 20$ mag, the radial completeness (lower panel of Fig. 5) is relatively flat above $0.5R_{200}$, and is, on average, 90%. In the internal region, it is slightly lower (80%) due to the possible fiber overlap and, mostly, to the lower priority given to targets already located inside the previous WINGS field of view.

The bottom panel takes into account the fact that the cluster-centric radial limit varies from cluster to cluster.

6. Velocity dispersions and memberships

The determination of cluster membership and of the cluster mean redshift is strictly related to the presence of possible interlopers in the cluster field of view. In our OmegaWINGS observations, this is even more problematic, given the very large field of view of our observations, that may be heavily contaminated by such objects in the external regions. In order to give a reliable estimate of these parameters, we therefore adopted an iterative procedure, as in Cava et al. (2009), following a $\pm 3\sigma$ clipping algorithm, first described by Yahil & Vidal (1977).

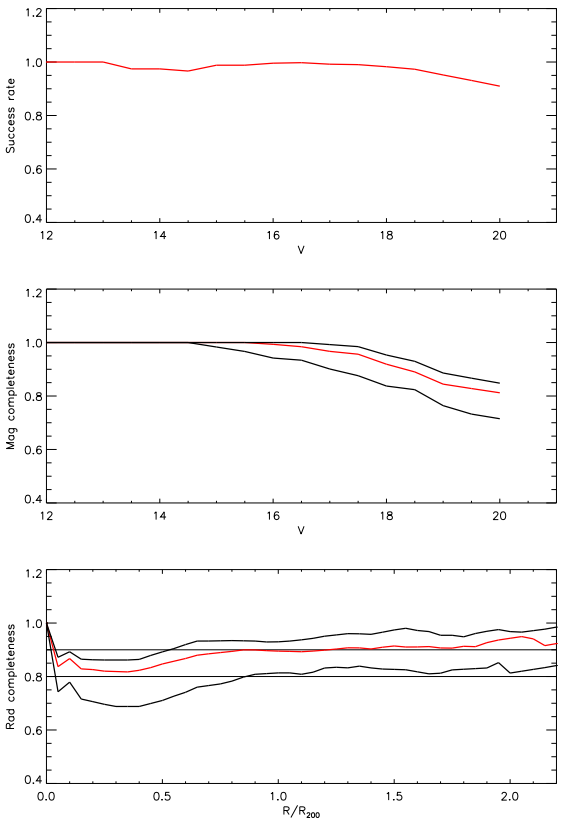

Fig. 5. *Upper panel*: success rate of redshift measurement. *Middle panel*: completeness in magnitude of the global OmegaWINGS spectroscopic sample. The red line gives the median value per bin of magnitude (in bins of 0.5 mag) and the two black lines represent the 15th and the 85th percentiles of the distribution. *Lower panel*: radial completeness.

The procedure starts by eliminating candidates whose velocities are outside a given fixed range (in our case those with $z > |z_{\rm cl} + 0.015|$). To this sample we apply an improved 3σ clipping, which includes the weighted gap method (e.g., Girardi et al. 1993) and interactively removes galaxies outside R_{200}. We proceed as follows.

Starting from the galaxies in the redshift range selected above and in the whole field of view with velocities given by $v = cz$, we apply the weighted gap method based on the ROSTAT routine (Beers et al. 1990), a widespread tool designed for robust estimation of simple statistics. Gaps are the measured gaps between the ordered velocities, here defined as $g_i = v_i + 1 - v_i$ for the sorted velocities, and weights as $w_i = i(N - i)$ for $i = 1, ..., N - 1$ for N galaxies. The weighted gap is defined as

$$\frac{\sqrt{gw}}{MM(\sqrt{gw})}, \tag{4}$$

where MM is defined as the mean of the central 50% of the data set and w_i are a set of approximately Gaussian weights. As stated in Beers et al. (1991), a weighted gap is considered significant if its value, relative to the mid mean of the other weighted gaps formed from the same sample, is greater than 2.25. In order to be conservative, we identified values larger than three as gaps, that thus suggest the possible presence of dynamical substructures altering the velocity dispersion determination. We visually inspected the velocity histograms to decide whether or not the gap found highlights the presence of a substructure and, if this is the case, galaxies identified as belonging to them have been removed

Table 3. OmegaWINGS main results.

Cluster	N_z	$N_{\rm memb,OW}$	$N_{\rm memb,tot}$	$z_{\rm cl}$	σ [km s^{-1}]	$\sigma_{\rm err}$ [km s^{-1}]	R_{200} Mpc	M_{200} 10^{15} $M_\odot$	$z_{\rm gap}$
A1069	496	107	130	0.0651	695	54	1.7	0.56	0.058
A151	623	165	248	0.0538	738	32	1.8	0.67	0.000
A1631a	673	288	369	0.0465	760	28	1.8	0.74	0.000
A168	459	141	141	0.0453	546	38	1.3	0.27	0.000
A193	239	72	101	0.0484	764	57	1.8	0.75	0.000
A2382	594	271	322	0.0639	698	30	1.7	0.57	0.069
A2399	678	234	291	0.0577	729	35	1.7	0.65	0.000
A2415	482	144	194	0.0578	690	37	1.7	0.55	0.000
A2457	535	232	249	0.0587	679	36	1.6	0.52	0.000
A2717	610	135	135	0.0498	544	46	1.3	0.27	0.000
A2734	556	220	220	0.0618	780	48	1.9	0.79	0.000
A3128	584	333	480	0.0603	838	28	2.0	0.98	0.000
A3158	621	243	357	0.0594	1023	37	2.5	1.79	0.069
A3266	877	479	678	0.0596	1318	39	3.2	3.82	0.000
A3376	519	229	263	0.0463	844	42	2.0	1.01	0.000
A3395	652	244	369	0.0507	1206	55	2.9	2.94	0.000
A3528	627	262	262	0.0545	1016	46	2.4	1.76	0.000
A3530	530	275	275	0.0548	674	38	1.6	0.51	0.000
A3532	250	107	107	0.0555	805	61	1.9	0.87	0.000
A3556	625	328	359	0.0480	668	34	1.6	0.50	0.000
A3558	706	442	442	0.0486	1003	33	2.4	1.69	0.000
A3560	580	244	283	0.0491	840	35	2.0	0.99	0.000
A3667	687	386	386	0.0558	1010	42	2.4	1.72	0.000
A3716	609	327	327	0.0457	848	26	2.0	1.02	0.000
A3809	695	189	244	0.0626	553	38	1.3	0.28	0.000
A3880	543	216	216	0.0580	688	56	1.7	0.54	0.000
A4059	686	229	229	0.0490	752	38	1.8	0.71	0.055
A500	478	187	227	0.0682	791	43	1.9	0.82	0.000
A754	423	250	338	0.0545	919	36	2.2	1.30	0.000
A85	359	172	172	0.0559	982	55	2.4	1.58	0.000
A957	154	48	92	0.0451	640	47	1.5	0.44	0.000
A970	331	136	214	0.0588	844	49	2.0	1.00	0.000
IIZW108	504	162	171	0.0486	611	38	1.5	0.38	0.000

Notes. For each cluster in Cols. (1)–(4), we give the number of redshifts derived from OmegaWINGS spectroscopy, the number of OmegaWINGS members and the total number of members (including WINGS results), respectively. Column (5) gives the estimated mean cluster redshift, while Cols. (6) and (7) are the velocity dispersion and its error, as derived from the number of members listed in Col. (4). Columns (8) and (9) are the R_{200} in Mpc and the M_{200} in units of 10^{15} $M_\odot$, respectively, while in the last column we show the secondary redshift (see Sect. 6 for details).

from the calculation of the cluster velocity dispersion. After the redefinition of structures, we computed the mean redshift $z_{\rm cl}$ and the rest frame velocity dispersion $\sigma_{\rm cl}$ for each cluster.

The following steps have then been iterated until convergence in $\sigma_{\rm cl}$ was reached: (1) based on the ROSTAT routine (see Beers et al. 1990), we used the biweight robust location and scale estimators to get $z_{\rm cl}$ and $\sigma_{\rm cl}$ and applied an iterative 3σ clipping until no rejection occurred; (2) we used the projected spatial distribution to define a further radius-dependent cut, that is, we determined R_{200} and removed galaxies outside this radius.

Once the mean cluster redshifts and the velocity dispersions had been determined, the memberships were derived for all galaxies, independently from the distances from the cluster center, here defined as the Brightest Cluster Galaxy (BCG). The redshifts and velocity dispersions that are given in Table 3 were derived using only redshifts from the OmegaWINGS and WINGS surveys, therefore excluding additional redshifts present in the literature. The errors quoted were obtained using the classical jackknife technique (Efron 1982).

In four of our clusters, the procedure used to derive the membership suggested the presence of another structure close but separated in velocity, with a slightly different redshift (shown in Table 3, last column). More details will be given in Biviano et al. (in prep.) where we will analyze additional structures and the presence of substructures within the clusters with a dedicated algorithm.

Figure 6 shows the redshift distribution for each cluster (in red), with the mean cluster redshift that we determined superimposed. Green histograms refer to galaxies belonging to the possible substructures.

In Table 3, we give the number of targets observed with AAOmega with a reliable redshift determination (Col. 2), the number of new cluster members (Col. 3), the total number of members (including the ones present only in the WINGS spectroscopic catalog) that contributed to the velocity dispersion determination (Col. 4), the velocity dispersion and its error in Cols. 5 and 6, and the R_{200} in Mpc. The R_{200} is the radius of the cluster region where the mean density is 200 times the critical density of the Universe, and has often been used as a proxy for the virial radius of a cluster.

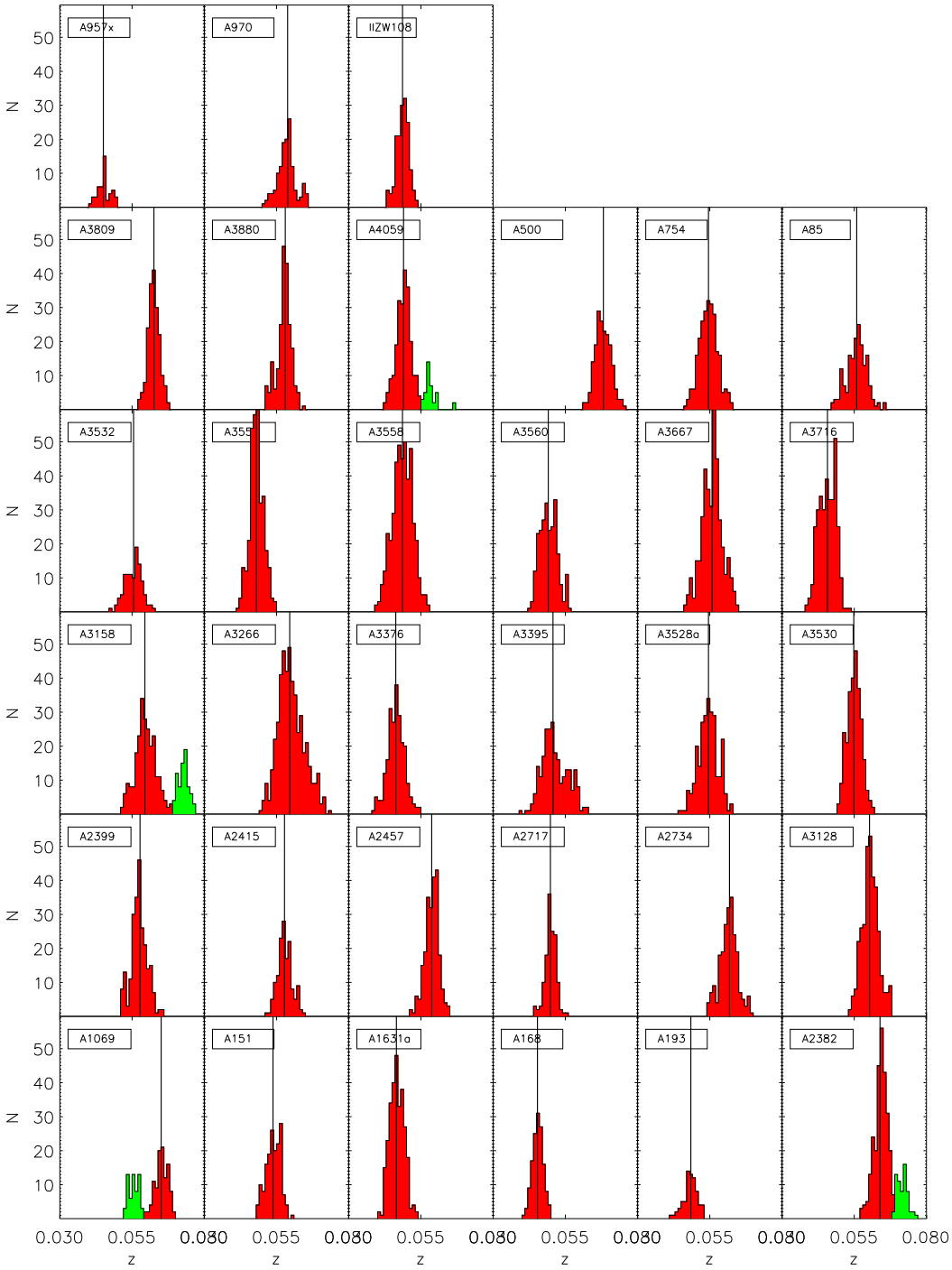

Fig. 6. Redshift distribution of the observed clusters as derived from the OmegaWINGS observations only. The vertical line shows the median cluster redshift (see Sect. 6 for the details). Green histograms refer to other probable structures close in velocity.

Following Poggianti et al. (2006), we calculated R_{200} as

$$R_{200} = 1.73 \frac{\sigma_{\rm cl}}{1000 \text{ km s}^{-1}} \frac{1}{\sqrt{\Omega_\Lambda + \Omega_0 (1+z_{\rm cl})^3}} h^{-1} \text{ Mpc}, \quad (5)$$

using the cluster velocity dispersion $\sigma_{\rm cl}$ and the cluster redshift $z_{\rm cl}$.

As a consequence, we derived the cluster masses (in 10^{15} $M_\odot$) as in Poggianti et al. (2006) using the relation between the cluster mass and the cluster velocity dispersion σ_v and redshift $z_{\rm cl}$ as in Finn et al. (2005), i.e.

$$M_{\rm cl} = 1.2 \left(\frac{\sigma_v}{1000 \text{ km s}^{-1}} \right)^3 \times \frac{1}{\sqrt{\Omega_\Lambda + \Omega_0 (1+z_{\rm cl})^3}} h_{100}^{-1} M_\odot \quad (6)$$

having adopted $H_0 = 70$, $\Omega_\Lambda = 0.7$ and $\Omega_0 = 0.3$.

Figure 7 shows the redshifts as a function of the distance from the cluster BCG (expressed in terms of R/R_{200}) for the OmegaWINGS clusters: red dots are the cluster members, while black ones are foreground/background galaxies. The horizontal line indicates the cluster redshift derived using the procedure

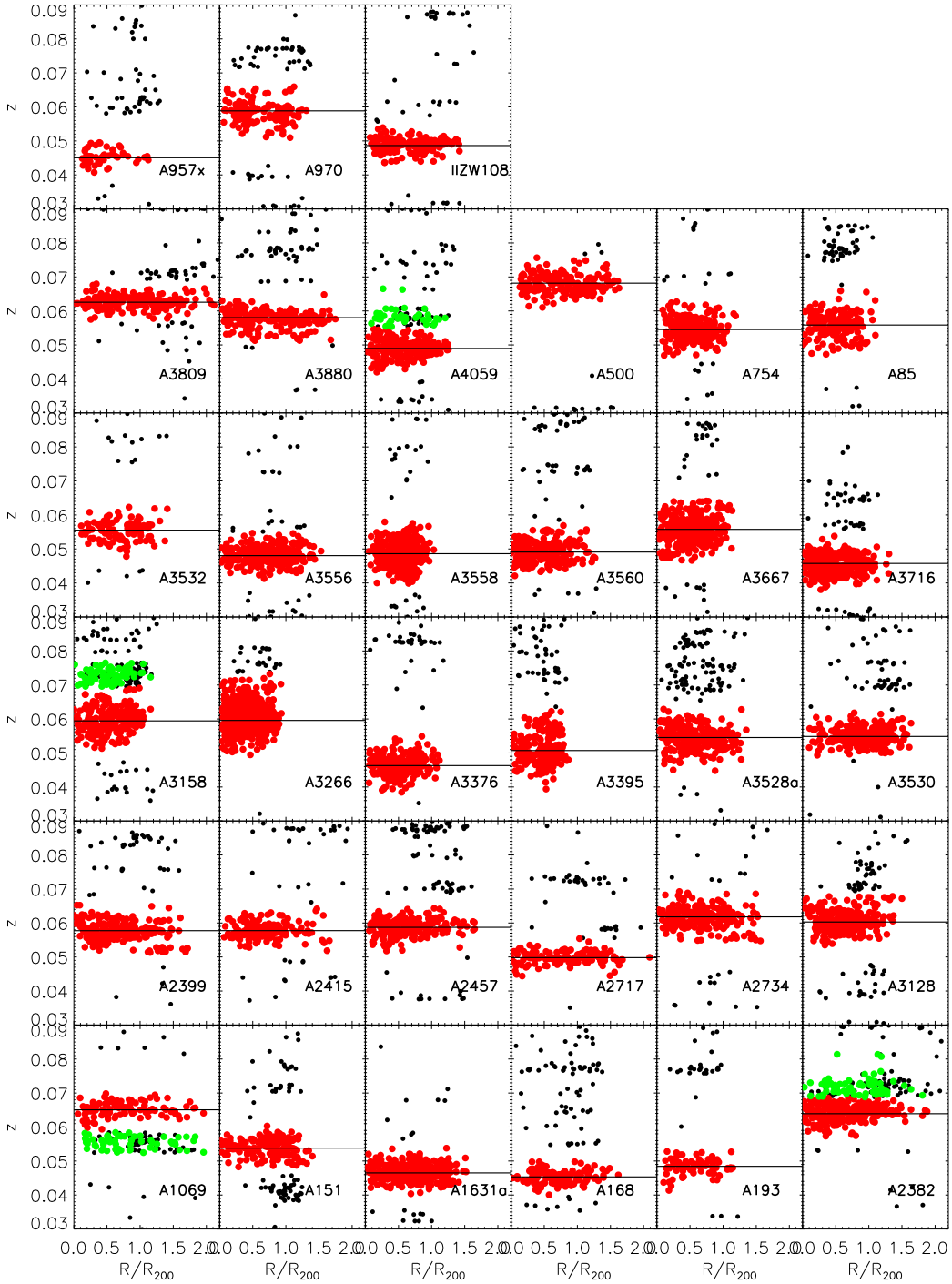

Fig. 7. Redshifts against distance from the cluster BCG, in terms of R/R_{200}. Red points show the cluster members, green points probable separate structures. Black dots are not members.

outlined above. For all clusters the OmegaWINGS surveys allows to reach at least the virial radius, and for some of them even a much larger region (out to $2 \times R_{200}$), where we still find cluster members.

Our estimates of cluster redshifts and velocity dispersions are in good agreement with those given by Cava et al. (2009), except for A3395, where we measure a much larger velocity dispersion (1206 km s^{-1} instead of 755 km s^{-1}). This could be due to the larger extent of the OmegaWINGS fields, that reaches in this case R_{200}, while the WINGS spectroscopic survey just reached $\sim 0.5 R_{200}$.

We show in Fig. 8 the sky distributions of OmegaWINGS cluster members (red dots) together with the R_{200} region (black circle), for each cluster. The green circles are galaxies that might be related to the secondary structures identified by the analysis of the redshift distribution only.

7. Access to the catalog

The complete catalog of OmegaWINGS redshift will be available at CDS and through the Virtual Observatory tool, as it is for the previous measurements derived from the

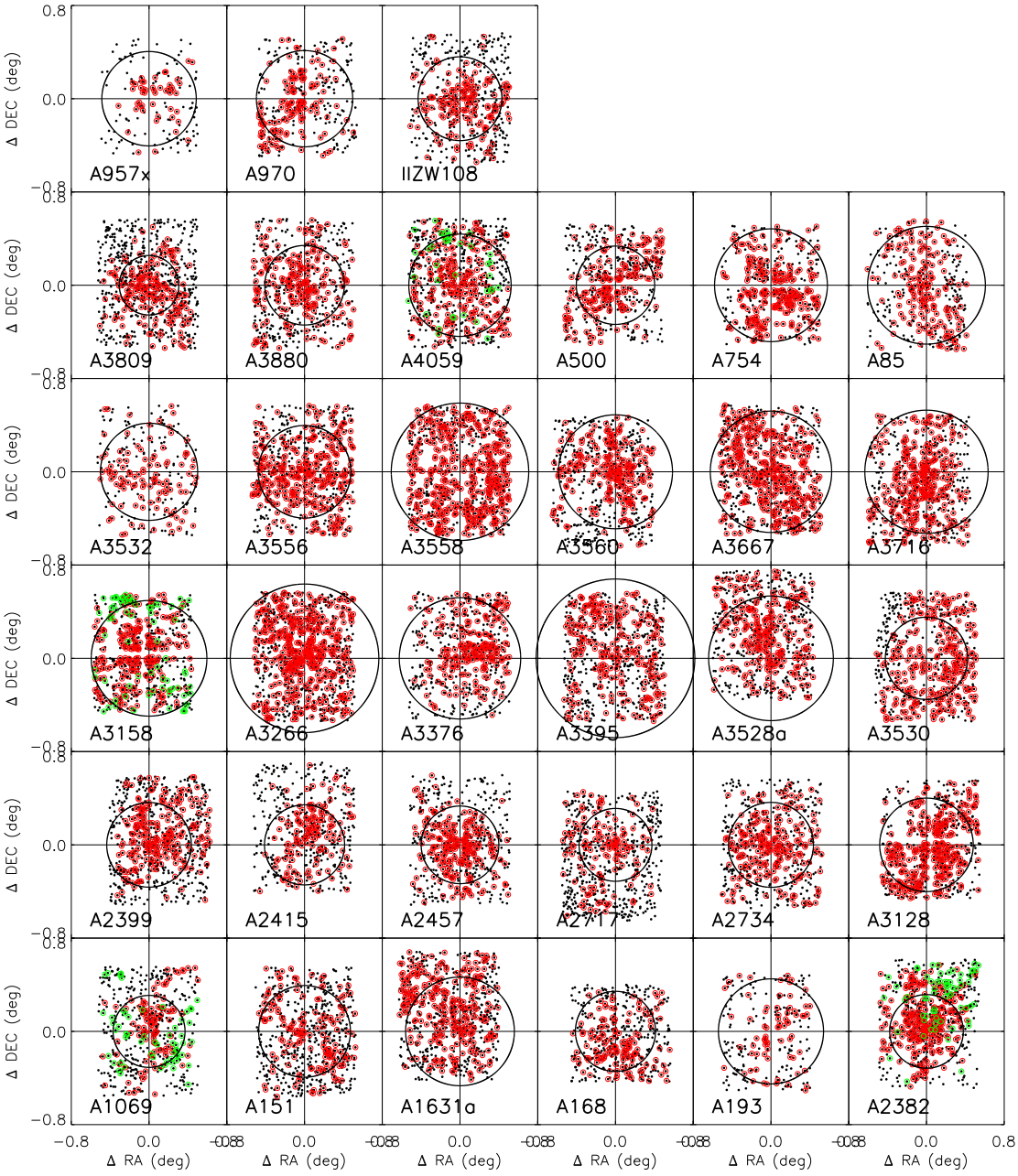

Fig. 8. Sky distribution of OmegaWINGS members (red symbols) and probable other structures (green symbols). Black dots are not members. The superimposed circle has a radius of R_{200}.

WINGS/OmegaWINGS dataset (see Moretti et al. 2014, for a complete description of the WINGS/OmegaWINGS database).

The WINGS identifier has been inherited from the photometric parent catalog by Gullieuszik et al. (2015), and it is unique inside the WINGS/OmegaWINGS database. We remind here that the identifier originates from the object coordinates, and that it has been newly assigned only when no match was present with sources already present in the original WINGS database (in order to avoid duplicates).

In the catalog, for each redshift, we give the OmegaWINGS identifier, the sky coordinates of the source, the redshift and its error, and the membership determined as previously described (flag 1 is for the galaxies considered cluster members, 0 for non-members). Galaxies flagged with membership 2 are those belonging to the other structures defined here on the basis of a secondary peak in the redshift distribution.

Radial and magnitude completeness were calculated as described in Sect. 5.1, and both must be taken into account when dealing with statistical studies, as we did in Vulcani et al. (2011a,b). OmegaWINGS spectra will be distributed in a forthcoming paper, where we will also give more details on the relative flux calibration and the spectrophotometric analysis.

8. Summary

In this paper, we present the redshift determination for 17 895 galaxies in $z = 0.04$–0.07 clusters as derived from observations obtained with the AAOmega spectrograph at AAT. Galaxies belong to 33 clusters out of the original 46 OmegaWINGS clusters observed with VST (Gullieuszik et al. 2015) over 1 square degree.

Table 4. OmegaWINGS redshifts.

Cluster	WINGS ID	RA (J2000)	Dec(J2000)	z	z_{err}	M compl	R compl	Memb
A1069	WINGSJ104034.89-083552.0	160.1454900	−8.5980600	0.17920	0.00064	0.788	0.789	0
A1069	WINGSJ104016.71-083547.4	160.0698700	−8.5968100	0.11306	0.00022	0.788	0.807	0
A1069	WINGSJ104105.27-083517.0	160.2719900	−8.5879700	0.05740	0.00016	0.788	0.842	2
A1069	WINGSJ104143.89-083206.8	160.4328900	−8.5352200	0.12495	0.00051	0.788	0.875	0
A1069	WINGSJ104042.94-083438.6	160.1788300	−8.5777400	0.09392	0.00046	0.788	0.797	0
A1069	WINGSJ104105.41-083212.3	160.2726900	−8.5367000	0.06503	0.00081	0.788	0.849	1
A1069	WINGSJ104027.03-083416.2	160.1127200	−8.5713900	0.09868	0.00012	0.788	0.789	0
A1069	WINGSJ104033.08-083146.9	160.1378900	−8.5299700	0.17782	0.00050	0.788	0.789	0
A1069	WINGSJ104123.59-082341.0	160.3482800	−8.3947100	0.21769	0.00019	0.788	0.875	0
A1069	WINGSJ104022.58-083037.8	160.0941500	−8.5107000	0.11511	0.00021	0.788	0.789	0
A1069	WINGSJ104017.22-083308.4	160.0718700	−8.5525100	0.11286	0.00042	0.788	0.789	0
A1069	WINGSJ104101.00-082438.1	160.2542400	−8.4106200	0.23828	0.00020	0.788	0.951	0
A1069	WINGSJ104130.86-081840.9	160.3786500	−8.3114000	0.26860	0.00022	0.788	0.778	0
A1069	WINGSJ104144.83-081515.6	160.4367800	−8.2543400	0.15127	0.00032	0.788	0.913	0
A1069	WINGSJ104106.03-082201.0	160.2751800	−8.3669600	0.31237	0.00046	0.788	0.900	0
A1069	WINGSJ104041.46-082648.1	160.1729400	−8.4469000	0.15228	0.00026	0.788	0.842	0
A1069	WINGSJ104026.93-082738.7	160.1123000	−8.4608300	0.31764	0.00025	0.788	0.797	0
A1069	WINGSJ104035.18-082746.3	160.1466100	−8.4630100	0.15894	0.00013	0.788	0.797	0
A1069	WINGSJ104138.64-080833.6	160.4110000	−8.1426700	0.06407	0.00008	0.788	1.000	1
A1069	WINGSJ104126.39-081046.8	160.3599500	−8.1796800	0.26871	0.00031	0.788	0.913	0

Notes. Column (1) gives the cluster name, Col. (2) the unique OmegaWINGS/WINGS identifier, Cols. (3) and (4), the sky coordinates in degrees, Cols. (5) and (6), the redshift and the relative error, Cols. (7) and (8), the completeness in magnitude and radial distance, respectively, and Col. (9), the membership. Cluster members are flagged 1 or 2, depending on the cluster structure/secondary structure, and 0 if they are not cluster members.

This sample of redshifts is aimed at giving a complete mapping of cluster galaxies out to large cluster-centric distances, that enables studies of galaxy transformations within clusters.

The high data quality expressed by the overall success rate of 95% in the redshift measurement, together with the radial and magnitude completeness (90% and 80% at $V = 20$ mag, respectively) characterize the sample as the most robust up to date for statistical studies of low-z cluster galaxies.

We have been able to determine new cluster redshifts and velocity dispersions, as well as cluster membership out to 1–2 virial radii depending on the cluster. 7497 galaxies turned out to be cluster members. Cluster masses derived using our velocity dispersions range from 2.7×10^{14} $M_{\odot}$ to 3.8×10^{15} $M_{\odot}$, therefore spanning a wide range in cluster properties.

Acknowledgements. Based on data acquired through the Australian Astronomical Observatory. We acknowledge financial support from PRIN-INAF 2014. B.V. acknowledges the support from an Australian Research Council Discovery Early Career Researcher Award (PD0028506). This research has made use of the SIMBAD database, operated at CDS, Strasbourg, France. We thank the anonymous referee for the helpful comments.

References

Barkhouse, W. A., Yee, H. K. C., & López-Cruz, O. 2007, ApJ, 671, 16
Beers, T. C., Flynn, K., & Gebhardt, K. 1990, AJ, 100, 32
Beers, T. C., Forman, W., Huchra, J. P., Jones, C., & Gebhardt, K. 1991, AJ, 102
Cava, A., Bettoni, D., Poggianti, B. M., et al. 2009, A&A, 495, 707
Dressler, A. 1980, ApJ, 236, 351
Efron, B. 1982, CBMS-NSF Regional Conference Series in Applied Mathematics (Philadelphia: Society for Industrial and Applied Mathematics)
Fasano, G., Marmo, C., Varela, J., et al. 2006, A&A, 445, 805
Fasano, G., Poggianti, B. M., Bettoni, D., et al. 2015, MNRAS, 449, 3927
Finn, R. A., Zaritsky, D., McCarthy, Jr., D. W., et al. 2005, ApJ, 630, 206
Girardi, M., Biviano, A., Giuricin, G., Mardirossian, F., & Mezzetti, M. 1993, ApJ, 404, 38
Gomez, P., Nichol, R., Miller, C., et al. 2003, ApJ, 584, 210
Gullieuszik, M., Poggianti, B., Fasano, G., et al. 2015, A&A, 581, A41
Haines, C. P., Merluzzi, P., Busarello, G., et al. 2011, MNRAS, 417, 2831
Jaffé, Y. L., Aragón-Salamanca, A., Kuntschner, H., et al. 2011, MNRAS, 417, 1996
Lewis, I., Balogh, M., De Propris, R., et al. 2002, MNRAS, 334, 673
Merluzzi, P., Mercurio, A., Haines, C. P., et al. 2010, MNRAS, 402, 753
Merluzzi, P., Busarello, G., Haines, C. P., et al. 2014, MNRAS, 446, 803
Miszalski, B., Shortridge, K., Saunders, W., Parker, Q. A., & Croom, S. M. 2006, MNRAS, 371, 1537
Moran, S. M., Miller, N., Treu, T., Ellis, R. S., & Smith, G. P. 2007, ApJ, 659, 1138
Moretti, A., Poggianti, B. M., Fasano, G., et al. 2014, A&A, 564, A138
Moretti, A., Bettoni, D., Poggianti, B. M., et al. 2015, A&A, 581, A11
Paccagnella, A., Vulcani, B., Poggianti, B. M., et al. 2016, ApJ, 816, L6
Pimbblet, K. A., Smail, I., Kodama, T., et al. 2001, MNRAS, 331, 333
Poggianti, B. M., von der Linden, A., De Lucia, G., et al. 2006, ApJ, 642, 188
Popesso, P., Biviano, A., Böhringer, H., & Romaniello, M. 2006, A&A, 445, 29
Sharp, R., & Parkinson, H. 2010, MNRAS, 408, 2495
Sharp, R., Saunder, W., Smith, G., et al. 2006, Ground-based and Airborne Instrumentation for Astronomy. eds. I. S. McLean, & M. Iye, Proc. SPIE, 6269
Smith, G. A., Saunders, W., Bridges, T., et al. 2004, in Ground-based Instrumentation for Astronomy. eds. A. F. M. Moorwood, & M. Iye. Proc. SPIE, 5492, 410
Smith, R. J., Lucey, J. R., Price, J., Hudson, M. J., & Phillipps, S. 2012, MNRAS, 419, 3167
Valentinuzzi, T., Woods, D., Fasano, G., et al. 2009, A&A, 501, 851
Valentinuzzi, T., Fritz, J., Poggianti, B. M., et al. 2010, ApJ, 712, 226
Vulcani, B., Poggianti, B. M., Aragón-Salamanca, A., et al. 2011a, MNRAS, 412, 246
Vulcani, B., Poggianti, B. M., Dressler, A., et al. 2011b, MNRAS, 413, 921
Vulcani, B., Poggianti, B. M., Fasano, G., et al. 2012, MNRAS, 420, 1481
Wenger, M., Ochsenbein, F., Egret, D., et al. 2000, A&AS, 143, 9
Yahil, A., & Vidal, N. V. 1977, ApJ, 214, 347
York, D. G. 2000, AJ, 120, 9